Photocatalysis of Dye-Sensitized TiO 2 Nanoparticles with Thin Overcoat of Al 2 O 3 : Enhanced Activity for H 2 Production and Dechlorination of CCl 4

ARTICLE *in* THE JOURNAL OF PHYSICAL CHEMISTRY C · JUNE 2009

Impact Factor: 4.77 · DOI: 10.1021/jp9008114

4 AUTHORS, INCLUDING:

Wonyong Choi

Pohang University of Science and Technol…

261 PUBLICATIONS **23,830** CITATIONS

SEE PROFILE

Photocatalysis of Dye-Sensitized TiO_2 Nanoparticles with Thin Overcoat of Al_2O_3: Enhanced Activity for H_2 Production and Dechlorination of CCl_4

Wooyul Kim,[†] Takashi Tachikawa,[‡] Tetsuro Majima,[‡] and Wonyong Choi*[,†]

School of Environmental Science and Engineering, Pohang University of Science and Technology (POSTECH), Pohang 790-784, Korea, and The Institute of Scientific and Industrial Research (SANKEN), Osaka University, Mihogaoka 8-1, Ibaraki, Osaka 567-0047, Japan

Received: January 27, 2009; Revised Manuscript Received: March 28, 2009

Dye-sensitized TiO_2 nanoparticles that were loaded simultaneously with Pt and Al_2O_3 overlayer (Al_2O_3/TiO_2/Pt) were synthesized and investigated for photocatalytic activity under visible light. Introducing a thin Al_2O_3 overlayer (~1 nm thick) on dye-sensitized TiO_2 markedly enhanced the visible light activities for the production of hydrogen (in the presence of EDTA as an electron donor) and the dechlorination of CCl_4. The Al_2O_3/TiO_2/Pt powder was characterized by HRTEM, EDX, and XPS. In agreement with the photocatalytic activity data, the photocurrent collected via electron shuttles on a Pt electrode immersed in an aqueous photocatalyst suspension under visible light was also enhanced in the presence of an Al_2O_3 overlayer, which indicates an enhanced interfacial electron transfer despite the presence of an insulating surface layer. The initial H_2 and chloride generation rate increased from 0.4 and 5 μM min^{-1} on TiO_2/Pt to 0.9 and 7.5 μM min^{-1} on Al_2O_3/TiO_2/Pt, respectively. The visible light activity of the sensitized photocatalytic reactions highly depended on the thickness of the alumina layer and was optimized at a low level of Al loading (Al/Ti atom ratio ~ 0.01), above which the activity was markedly reduced with thickening of the layer. It is suggested that the alumina layer retards the charge recombination between the electron injected from the excited dye and the oxidized dye. The slower charge recombination in the presence of an alumina overlayer was confirmed by time-resolved diffuse reflectance (TDR) spectroscopy.

Introduction

Solar energy conversion through semiconductor photocatalysis needs to maximize the utilization of visible light, and the dye sensitization of oxide semiconductors has been intensively studied for this purpose.[1−3] In particular, dye-sensitized TiO_2 is the most popular and successful for solar cell applications.[4−7] It has been also applied to visible-light-induced hydrogen production[8−12] and pollutant degradation[13−17] in aqueous solutions. The essence of dye sensitization is the electron injection from the excited dye to the conduction band (CB) of TiO_2 and the subsequent interfacial electron transfer. The main pathways are illustrated in Scheme 1.

The overall sensitization efficiency is maximal if all injected electrons are transferred to electron-accepting substrates (e.g., proton/water for hydrogen production, chlorinated organic compounds for reductive dechlorination). However, the recombination (path 5 in Scheme 1) between the injected electron and the oxidized dye reduces the overall efficiency. This short-circuiting path is particularly predominant when the semiconductor particles are isolated in the dispersed state (e.g., colloid, suspension), whereas those in the thin film state (e.g., dye-sensitized solar cell) are well connected for the migration of injected electrons to minimize the recombination. Many different approaches have been tried to solve this problem. For example, depositing Pt nanoparticles on the dye-sensitized TiO_2 surface highly enhances the visible photocatalytic activity by competitively scavenging electrons into the metal phase (Schottky barrier electron trapping).[18,19] Another approach is to coat a thin overlayer of insulating oxides (e.g., Al_2O_3) on the surface of TiO_2. Such an approach was successfully demonstrated for a dye-sensitized solar cell (DSSC) in which the oxide overlayer acts as a barrier layer for the recombination process (path 5).[5,6] Although the presence of the barrier layer on TiO_2 slows down not only the recombination process but also the electron injection (path 2), the latter yield was little influenced by the presence of the barrier layer in DSSC due to the extremely fast dynamics of the electron injection.[5,6] Incidentally, it was also reported that

SCHEME 1: Schematic Illustration of Electron Transfer/Recombination Processes Occurring on a Dye-Sensitized TiO_2 Particle with Al_2O_3 Overlayer for (a) H_2 Production and (b) CCl_4 Dechlorination[a]

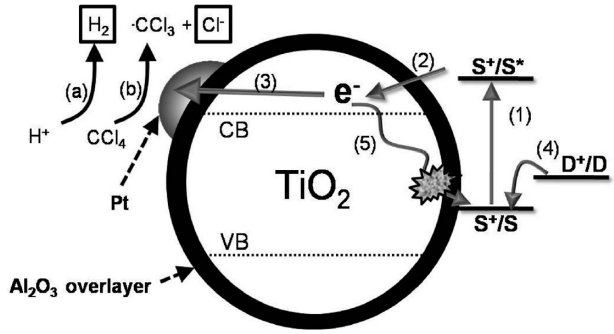

[a] The numbered paths indicate the following: (1) dye excitation; (2) electron injection from the excited dye to TiO_2 CB; (3) electron trapping on Pt; (4) regeneration of the oxidized dye by electron donor (D); (5) back electron transfer to the oxidized dye (recombination).

* Corresponding author. Fax: +82-54-279-8299. E-mail: wchoi@postech.edu.
[†] POSTECH.
[‡] Osaka University.

10.1021/jp9008114 CCC: $40.75
Published on Web 05/21/2009

Al_2O_3-coated TiO_2 enhanced the sensitized degradation of dyes under visible light by adsorbing the dye preferentially on Al_2O_3.[15]

In this work, we prepared dye-sensitized TiO_2 nanoparticles that were loaded simultaneously with Pt nanoparticles and Al_2O_3 overlayer ($Al_2O_3/TiO_2/Pt$) and tested the visible light activity for hydrogen production and the dechlorination of CCl_4 in aqueous suspensions. Although both test reactions should be initiated by the interfacial transfer of CB electrons on TiO_2, the presence of insulating alumina overlayer significantly enhanced the visible light activity in both cases. The enhanced photocatalytic activities imply that the charge recombination in the dye-sensitized TiO_2 should be retarded by the alumina overlayer, which was monitored and confirmed by time-resolved diffuse reflectance spectroscopy.[20−23]

Experimental Section

Materials and Chemicals. TiO_2 with an alumina overlayer was synthesized by a sol−gel process. A commercial TiO_2 sample (Degussa P25) was compared when needed. Ruthenium bipyridyl complexes with a carboxylate anchoring group, $Ru^{II}(4,4\text{-}(CO_2H)_2bpy)_3$ (abbreviated as $Ru^{II}L_3$; bpy is 2,2-bipyridine), were synthesized according to our previous studies[10,14] and used as the sensitizer in this study. Titanium isopropoxide (Junsei, 98%), aluminum isopropoxide (Aldrich, 99.99%), chloroplatinic acid ($H_2PtCl_6 \cdot 6H_2O$) (Aldrich), 2-propanol (Aldrich), ethylenediaminetetraacetic acid (EDTA, Aldrich), ammonium hydroxide (Aldrich), and $FeCl_3 \cdot 6H_2O$ (>99%, Kanto) were used as received. CCl_4 (Aldrich) was purified by distillation. A saturated stock solution of CCl_4 (5 mM) was prepared by stirring excess CCl_4 into deoxygenated distilled water. $HClO_4$ and NaOH were used for the pH adjustment of aqueous suspensions. The deionized water used was ultrapure (18 MΩ·cm) and was prepared by a Barnstead purification system.

Synthesis and Characterization of $Al_2O_3/TiO_2/Pt$ Photocatalysts. The Al_2O_3-overcoated TiO_2 was synthesized through a sol−gel process according to a literature method.[16] Titanium isopropoxide and appropriate amounts of aluminum isopropoxide (Al/Ti atom ratio = 0, 0.005, 0.009, 0.018, 0.09, and 0.18) were dissolved in 2-propanol. The resulting solution was added dropwise to 0.3 M nitric acid solution in an ice/water bath under vigorous stirring and then the pH was adjusted to ca. 9 with ammonium hydroxide. After aging for 2 h, the resulting white gel was thoroughly washed, dried, and calcined at 450 °C for 3 h. After grinding, the calcined catalysts were washed with water again and dried at 100 °C under vacuum overnight. Al_2O_3 was synthesized through the same procedure without titanium isopropoxide.

Platinum nanoparticles were loaded onto Al_2O_3/TiO_2 and TiO_2 particles using a photodeposition method.[24,25] The platinization was carried out in an aqueous suspension of Al_2O_3/TiO_2 or TiO_2 (0.5 g/L) in the presence of methanol (electron donor, 1.25 M) and chloroplatinic acid (H_2PtCl_6, 2.57 μM) under UV irradiation for 30 min (with a 200-W mercury lamp). After irradiation, the platinized catalysts ($Al_2O_3/TiO_2/Pt$ or TiO_2/Pt) were filtered and washed with distilled water. A typical Pt loading was estimated to be ca. 0.1 wt %.

The high-resolution transmission electron micrographs (HR-TEM) and energy-dispersive X-ray (EDX) analysis of $Al_2O_3/TiO_2/Pt$ and TiO_2/Pt were obtained using a JEM-2100F microscope with Cs correction. X-ray photoelectron spectra (XPS, Kratos XSAM 800pci) of $Al_2O_3/TiO_2/Pt$ and TiO_2/Pt powders were obtained using the Mg Kα line (1253.6 eV) as the excitation source.

Photolysis and Analysis. $Al_2O_3/TiO_2/Pt$ or TiO_2/Pt powder was redispersed in distilled water (0.5 g/L) under sonication, and then the ruthenium sensitizer ($Ru^{II}L_3$) was added. The typical concentration of the dye sensitizer added to the suspension was 8.3 μM. The dye oxidized after electron injection can be regenerated by suitable electron donors (EDTA in H_2 production[10] and water in CCl_4 dechlorination[14,19]). The sensitizer adsorption on $Al_2O_3/TiO_2/Pt$ (or TiO_2/Pt) was achieved by adding the catalyst in the aqueous sensitizer solution and the subsequent equilibration for 0.5 h. At pH 3, all added sensitizer molecules were quantitatively adsorbed on the surface of catalysts. The UV−visible absorption and emission spectra showed no sign of sensitizers present in the filtrate (through a 0.45 μm PTFE filter) of the equilibrated sensitizer-added suspension of TiO_2 whether the alumina overlayer was present or not. All experiments in this work were carried out at pH 3. The reactor with the catalyst suspension was bubbled with N_2 for 30 min to remove the dissolved oxygen prior to irradiation.

The visible light activities of $Ru^{II}L_3$-sensitized $Al_2O_3/TiO_2/Pt$, TiO_2/Pt, and P25/Pt powders were tested for photoreductive dechlorination of CCl_4 and H_2 production. The two reduction tests were separate ones that were carried out under different experimental conditions. A 300-W Xe arc lamp (Oriel) combined with a 10-cm IR water filter and a cutoff filter ($\lambda > 420$ nm for visible light irradiation) was used as a light source, and then the filtered light was focused onto a reactor (30 mL for CCl_4 dechlorination or 50 mL for H_2 production) with a quartz window. A typical incident light intensity was measured using a power meter (Newport 1830-C) and determined to be about 100 mW/cm^2 in the wavelength range 420−550 nm that overlaps with the major absorption band of $Ru^{II}L_3$. As for the H_2 production experiment, the aqueous solution containing Pt/TiO_2, $Ru^{II}L_3$ (8.3 μM), and EDTA (10 mM) at pH 3 was deaerated by N_2 sparging. The production of H_2 under irradiation was monitored using a gas chromatograph (HP6890A) equipped with a thermal conductivity detector and a 5A molecular sieve column. For CCl_4 dechlorination, the catalyst suspension (without EDTA, deaerated) was added with CCl_4. A calculated amount of CCl_4 stock solution was injected into the reactor with a gastight syringe through a rubber septum. A typical concentration of CCl_4 was 1 mM. Sample aliquots were withdrawn by a 1-mL syringe intermittently during the photoreaction and filtered through a 0.45-μm PTFE filter (Millipore) to remove suspended catalyst particles. The analysis of chlorides generated from CCl_4 dechlorination was performed using an ion chromatograph (IC, Dionex DX-120), which was equipped with a Dionex IonPac AS14 (4 mm × 250 mm) column and a conductivity detector. The eluent solution was 3.5 mM Na_2CO_3/1 mM $NaHCO_3$. Duplicate experiments were carried out under the identical condition to confirm the reproducibility.

Photoelectrochemical Measurements. The photocurrents were collected via electron shuttles on an inert electrode (Pt) immersed in aqueous suspensions of sensitized TiO_2/Pt or $Al_2O_3/TiO_2/Pt$ under visible light illumination.[26] Catalyst (0.5 g/L), $Ru^{II}L_3$ (sensitizer), EDTA (electron donor), and Fe^{3+} (reversible electron shuttle) were added in distilled water, and the suspension pH was adjusted to 2.00 ± 0.05 with $HClO_4$. A platinum plate (1 × 1 cm^2), Ag/AgCl, and a graphite rod were immersed in the reactor as a working

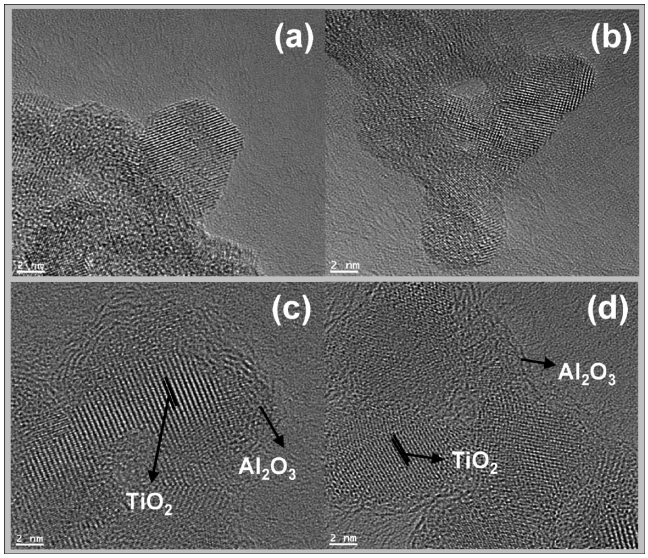

Figure 1. High-resolution TEM images of TiO_2/Pt (a, b) and Al_2O_3/TiO_2/Pt (c, d).

(collector), a reference, and a counter electrode, respectively. Nitrogen gas (>99.9%) was continuously purged through the suspension. Photocurrents were collected in the suspension by applying a potential (+0.573 V vs Ag/AgCl) to the Pt working electrode using a potentiostat (Gamry, Reference 600) connected to a computer. The suspension was magnetically stirred throughout the photocurrent measurements.

Time-Resolved Diffuse Reflectance (TDR) Measurements. The TDR measurements were performed using the third harmonic generation (355 nm, 1.5 mJ/pulse, 5 ns full width at half-maximum (fwhm)) and the second harmonic generation (532 nm, 2.0 mJ/pulse, 5 ns fwhm) from a Q-switched Nd^{3+}:YAG laser (Continuum, Surelite II-10) for the excitation operated with temporal control by a delay generator (Stanford Research Systems, DG535).[21−23] The reflected analyzing light from a pulsed 450-W Xe arc lamp (Ushio, UXL-451-0) was collected by a focusing lens and directed through a grating monochromator (Nikon, G250) to a silicon avalanche photodiode detector (Hamamatsu Photonics, S5343). The transient signals were recorded by a digitizer (Tektronix, TDS 580D). The reported signals were the averages of 30−100 events. The aqueous slurry (pH 3) for the TDR measurements contained the catalyst powder (20 g/L) and $Ru^{II}L_3$ (33 μM). All experiments were carried out at room temperature.

Results and Discussion

Characterization of Al_2O_3/TiO_2/Pt. The HRTEM images of TiO_2/Pt and Al_2O_3/TiO_2/Pt are compared in Figure 1. The lattice fringes in both images show the (103) crystallographic planes of anatase from the standard diffraction pattern of TiO_2 (JCPDS 21-1272). While the image of TiO_2/Pt shows that the crystalline portion of TiO_2 is extended to the particle boundary, the thin amorphous Al_2O_3 overlayer on TiO_2 crystallites is observed in the Al_2O_3/TiO_2/Pt sample. The presence of the Al_2O_3 overlayer was found in all particles, with thicknesses of about 5−10 Å. Such HRTEM images that show the alumina layers capped on TiO_2 were also shown in other related studies which employed Al_2O_3/TiO_2.[6,16] Since the Pt content was very low (0.1 wt %), the size of Pt particles could not be determined from the HRTEM images. The EDX image analysis clearly exhibits Al and Pt elemental spots within the Al_2O_3/TiO_2/Pt particles (Figure 2). The Al elements

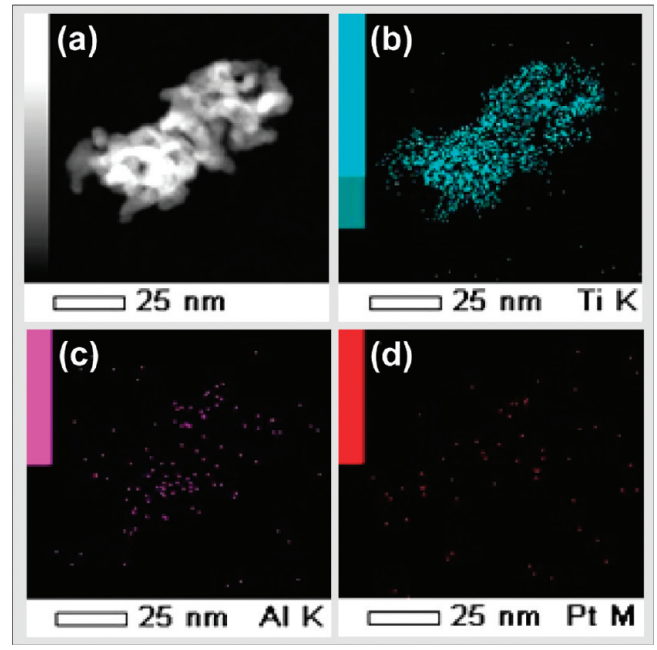

Figure 2. Energy-dispersive X-ray images of (a) high-angle annular dark field image and the elemental mapping of (b) Ti, (c) Al, and (d) Pt on Al_2O_3/TiO_2/Pt sample. Al/Ti atom ratio = 0.018.

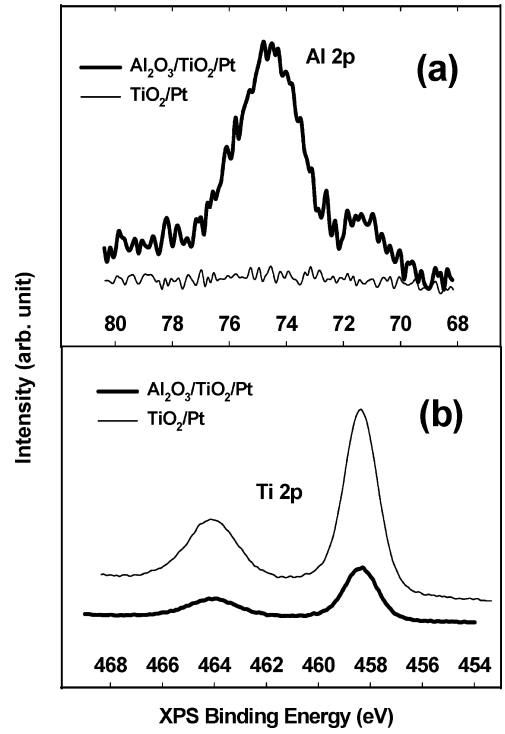

Figure 3. XPS spectra of Al_2O_3/TiO_2/Pt and TiO_2/Pt powder in the (a) Al 2p and (b) Ti 2p band regions.

are rather scattered over the titania support. Although the simplified illustration of Scheme 1 shows that the surface of TiO_2 is completely covered with the alumina layer, a more realistic representation may be the TiO_2 surface patched with alumina islands. Figure 3 compares the XPS spectra of Al_2O_3/TiO_2/Pt and TiO_2/Pt in the Al 2p and Ti 2p bands. The Al 2p band of Al_2O_3/TiO_2/Pt was positioned at 74.4 eV, which exactly matches that of Al 2p in pure Al_2O_3 (74.4 eV).[27] The intensity of the Ti 2p band in Al_2O_3/TiO_2/Pt was reduced because of the presence of Al_2O_3 overlayer, but the Ti 2p

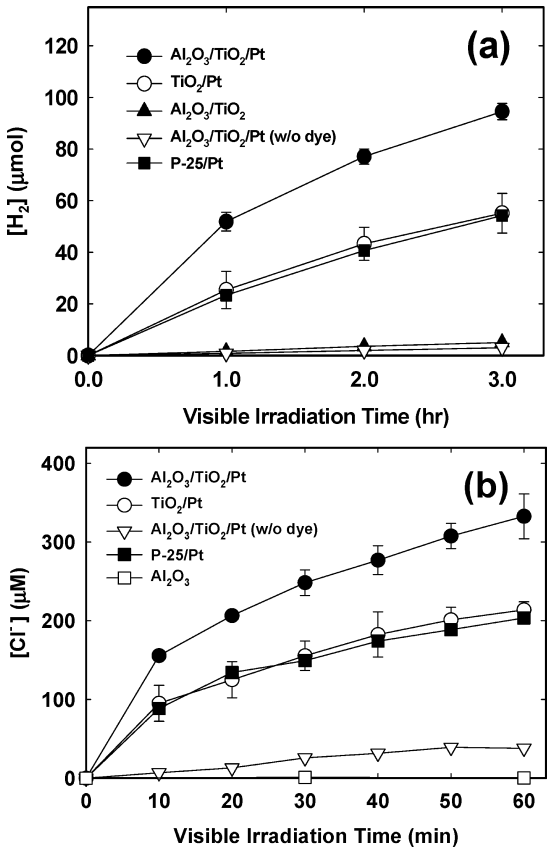

Figure 4. Time-dependent profiles of (a) hydrogen generation and (b) chloride production from CCl_4 degradation in visible-light-irradiated suspensions of $Ru^{II}L_3$-sensitized P25/Pt, TiO_2/Pt, Al_2O_3/TiO_2, and Al_2O_3/TiO_2/Pt. The experimental conditions were [catalyst] = 0.5 g/L, $[Ru^{II}L_3]$ = 8.3 μM, Al/Ti atom ratio = 0.009, pH_i = 3, [EDTA] = 10 mM (for (a) H_2 generation), $[CCl_4]$ = 1 mM (for (b) Cl^- generation), initially N_2-saturated, and $\lambda > 420$ nm irradiation.

binding energy (464.34, 458.8 eV) in both Al_2O_3/TiO_2/Pt and TiO_2/Pt was identical to that of pure TiO_2.[27]

Activity of Dye-Sensitized Al_2O_3/TiO_2/Pt. The photocatalytic reactions occurring on the dye-sensitized TiO_2 mainly follow reductive pathways since they are initiated by the electrons injected from the excited dye (reaction 1). Two reductive reactions (reactions 2 and 3) were tested in this study. Figure 4a shows the time-dependent profile of hydrogen production (reaction 2) in the visible-light-illuminated suspension of dye-sensitized TiO_2/Pt and Al_2O_3/TiO_2/Pt. The presence of the Al_2O_3 barrier layer clearly enhanced the $Ru^{II}L_3$-sensitized production of hydrogen. No hydrogen was produced in the absence of dye or platinum loading. The sensitized activity of Al_2O_3/TiO_2 was also higher than that of a popular commercial TiO_2 (P25).

$$Ru^{II}L_3^* \text{ (on } TiO_2) \rightarrow e_{cb}^- + Ru^{III}L_3 \quad (1)$$

$$e_{cb}^- + H^+ \rightarrow 1/2H_2 \quad (2)$$

$$e_{cb}^- + CCl_4 \rightarrow {}^{\bullet}CCl_3 + Cl^- \quad (3)$$

In a similar way, the visible-light-sensitized dechlorination of CCl_4 (reaction 3) was also clearly enhanced when the Al_2O_3 barrier layer was present on TiO_2 as shown in Figure 4b. The initial chloride generation rate increased from 5 μM min^{-1} on both TiO_2/Pt and P25/Pt to 7.5 μM min^{-1} on Al_2O_3/TiO_2/Pt. The control test of dye/Al_2O_3 showed no activity for CCl_4 dechlorination, which confirmed that the dye on an inert support cannot sensitize CCl_4 at all. Since both hydrogen production and dechlorination of CCl_4 proceed through the interfacial electron transfer, the barrier-assisted inhibition of the recombination path (reaction 4) should enhance the overall sensitization process.

$$e_{cb}^- + Ru^{III}L_3 \rightarrow Ru^{II}L_3 \quad (4)$$

Compared with the total number of $Ru^{II}L_3$ sensitizer molecules (0.25 μmol) adsorbed on Al_2O_3/TiO_2/Pt in the reactor, the numbers of H_2 molecules and Cl^- ions generated in the reactor were 97 μmol (in 3 h) and 10 μmol (in 1 h), respectively. This clearly indicates that the sensitizer molecules are catalytic and the oxidized sensitizers after the electron injection should be regenerated by suitable electron donors (EDTA in H_2 production and water in CCl_4 dechlorination). Incidentally, the dye molecules may be adsorbed on TiO_2 as well as Al_2O_3 surface because the surface of Al_2O_3/TiO_2/Pt catalyst may not be completely covered with the alumina as we mentioned previously. However, the ruthenium dye seems to be more preferably adsorbed on Al_2O_3. It has been reported that rhodamine B (a dye with a carboxylate anchoring group like the ruthenium complex) preferentially adsorbed on Al_2O_3 rather than Ti(IV) sites on the surface of Al_2O_3/TiO_2 catalyst that was prepared by the same method as the present one.[16] We also measured and compared the adsorption isotherms of $Ru^{II}L_3$ on the suspended catalysts of bare TiO_2 and Al_2O_3/TiO_2 (data not shown). Although the adsorption of the ruthenium dye is the same between the two catalysts at lower dye concentrations (<30 μM), the dye adsorption on Al_2O_3/TiO_2 was 2 times that on bare TiO_2 at $[Ru^{II}L_3]_0$ = 100 μM.

The presence of insulating Al_2O_3 overlayer on TiO_2 should influence (i.e., retard) all reactions 1−4 in which the electron transfer is involved, but the degree of the retardation should vary from reaction to reaction. The retardation of reactions 1−3 should reduce the overall sensitization efficiency, but that of reaction 4 has the opposite effect. The fact that the net effect of the barrier layer loading was positive indicates that the extent of the retardation of the recombination (reaction 4) outweighs the retardation effect for reactions 1−3.

Fe^{3+}-Mediated Photocurrent Collection. To confirm the effect of Al_2O_3 overlayer on the electron transfer, we measured photocurrents collected on an inert Pt electrode immersed in the aqueous suspension of TiO_2/Pt or Al_2O_3/TiO_2/Pt under visible light. The redox couple of Fe^{3+}/Fe^{2+} was used as an electron shuttle that carries the electron from the conduction band (CB) of TiO_2 to the Pt collector electrode as follows.[26]

$$e_{cb}^- + Fe^{3+} \rightarrow Fe^{2+} \quad (5)$$

$$Fe^{2+} \rightarrow Fe^{3+} + Pt(e^-) \quad (6)$$

The collected current is a direct indicator of the transfer of CB electrons, and the higher current implies that the steady-state concentration of CB electrons in TiO_2 particles is higher. The visible-light-induced photocurrent generation profiles are compared in Figure 5. In agreement with the photocatalytic activity data, the collected current is higher when there is an Al_2O_3

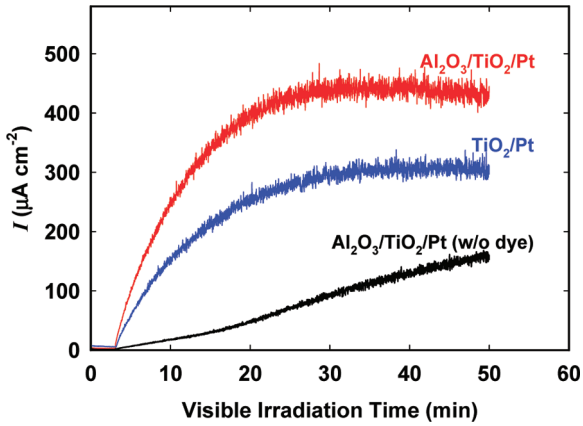

Figure 5. Time-dependent profiles of Fe^{3+}-mediated photocurrent collected on a Pt electrode in visible-light-irradiated suspensions of sensitized TiO_2/Pt and Al_2O_3/TiO_2/Pt. The experimental conditions were [catalyst] = 0.5 g/L, $[Ru^{II}L_3]$ = 8.3 μM, Al/Ti atom ratio = 0.009, pH_i = 2, [EDTA] = 10 mM, $[Fe^{3+}]$ = 1 mM, continuously N_2-purged, and $\lambda > 420$ nm irradiation.

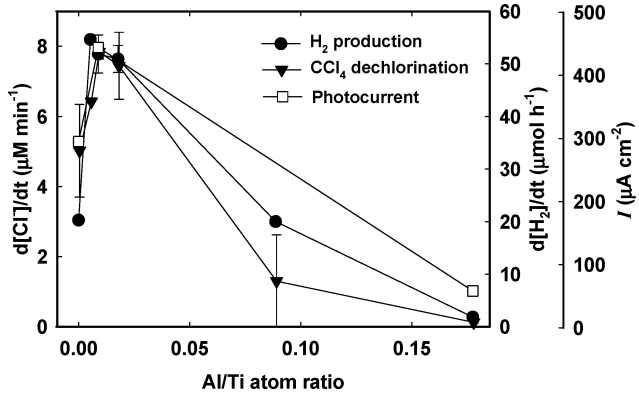

Figure 6. Effect of Al_2O_3 overlayer thickness (in terms of Al/Ti atom ratio) on initial rate of hydrogen generation, initial rate of chloride production from CCl_4 degradation, and photocurrent collected in the suspension under visible light (after 50 min irradiation).

overlayer. This confirms that the presence of the barrier layer enhances the steady-state concentration of CB electrons in suspended TiO_2 particles under irradiation. The higher concentration of CB electrons due to the hindered recombination should lead to the enhanced interfacial electron transfer.

Effect of Barrier Layer Thickness. The sensitized photocatalytic reactions should depend on the thickness of the barrier layer. When the barrier layer is too thick, the electron from the excited dye cannot efficiently tunnel through the barrier layer into CB of TiO_2. Figure 6 shows the effect of the Al_2O_3 loading (in terms of Al/Ti atom ratio) on the sensitized photocatalytic activity and the photocurrent collection. For all three systems, the activity dependence on the Al_2O_3 loading is very similar. The overall sensitization efficiency rapidly increases with the alumina loading and then reaches a maximum beyond which the efficiency decreases with increasing the barrier layer loading. The optimal loading was found at Al/Ti = 0.009−0.018, and the activity was insignificantly low at Al/Ti = 0.18.

Recombination Dynamics through Time-Resolved Diffuse Reflectance Spectroscopy. The effect of the barrier layer on the charge recombination dynamics can be directly probed by TDR spectroscopy. Although the primary role of the Al_2O_3 layer is to provide an insulating barrier to retard the back electron transfer, it may induce other side effects. For

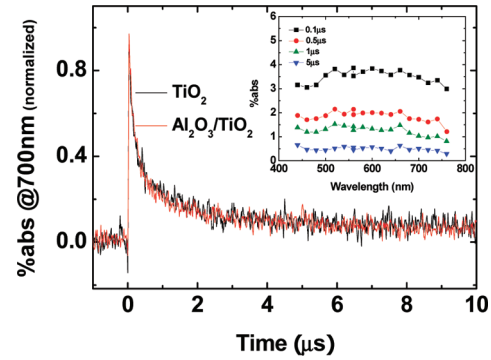

Figure 7. Normalized time traces of absorbance at 700 nm during the 355-nm laser photolysis of bare TiO_2 and Al_2O_3/TiO_2 in slurry. Inset: TDR spectra during the 355-nm laser photolysis of Al_2O_3/TiO_2. The % absorption (%abs) is given by the equation %abs = $(R_0 - R)/R_0 \times 100$, where R and R_0 represent the intensities of the diffuse reflected monitor light with and without excitation, respectively.[21−23]

example, the presence of Al_2O_3 on the interface with TiO_2 may create defect sites in the band gap and influence the charge transfer dynamics. To test such a possibility, the charge carriers generated during the 355-nm laser (UV) irradiation of bare TiO_2 and Al_2O_3/TiO_2 (without dyes) were monitored. The inset of Figure 7 exhibits that the laser excitation of Al_2O_3/TiO_2 generates the broad transient absorption band in the 440−800 nm range which represents the overlapping of the trapped h^+ (440−650 nm) and trapped e^- (550−800 nm). This spectral feature of the transient absorption of Al_2O_3/TiO_2 is very similar to that of bare TiO_2 (data not shown) and consistent with the literature data.[28−31] Figure 7 compares the time profiles of the transient absorption decay between bare TiO_2 and Al_2O_3/TiO_2. The absorbance decay profiles monitored at 550 nm (for trapped hole) and 700 nm (for trapped electron) show no difference between the two photocatalysts, which suggests that the presence of the alumina overlayer does not introduce defect sites that affect the major charge recombination dynamics in TiO_2 lattice. This also implies that the interfacial electron transfer process occurring on the dye-sensitized Al_2O_3/TiO_2 should not be interfered with by the potential defect sites created by the alumina loading.

On the basis of the premise that the major band structure and energy levels in TiO_2 remain unaffected by the presence of a thin overlayer of Al_2O_3 (as argued above), the electron transfers between TiO_2 (or Al_2O_3/TiO_2) and dye can be indirectly followed by monitoring the transient absorbance of the dyes and dye cations after a visible laser pulse excitation. We monitored the transient bleaching of the ground-state dye absorbance (460 nm) and the transient absorbance of the dye cation (650 nm)[32,33] and trapped electron (550−800 nm)[28−31] during the 532-nm laser photolysis of dye-sensitized bare TiO_2 and Al_2O_3/TiO_2. As shown in Figure 8a, the dye bleaching (or the electron injection) was completed within the laser pulse scattering (80 ns) and the bleached dye was recovered in 30 μs. The accompanying dye cations also appeared within the laser pulse and decayed along with the recovery of the bleached dye. A significant fraction of the absorbance at $\lambda > 600$ nm remained after 30 μs, although the bleached dye was apparently recovered within the same time domain. The residual absorbance at $\lambda >$ 600 nm should be ascribed not only to the long-lived dye cations but also to the trapped electrons since the absorption spectrum of the dye cation overlaps with that of the trapped electrons. The observed time traces were well reproduced using a stretched exponential function:[34]

$$\%\text{abs} = (\%\text{abs})_0 \exp[-(t/\tau)^{\alpha}] \quad (7)$$

where $(\%\text{abs})_0$ is the initial absorbance of the dye cations that were generated within the laser pulse (at $t = 0$), τ is the average lifetime, and α is the heterogeneous parameter. The fitting parameters are summarized in Table 1. The $(\%\text{abs})_0$ value was not reduced with Al_2O_3/TiO_2. An increase in τ by about 3 times in the presence of Al_2O_3 layer supports the idea that the barrier layer slows down the recombination. A slight increase in α might be attributed to a shift from electron transport limited charge recombination to more interfacial electron transfer limited dynamics as suggested elsewhere.[34]

The time-resolved decay of the dye cation (Figure 8b) was moderately retarded with Al_2O_3/TiO_2 compared with bare TiO_2, which supports the idea that the barrier layer slows down the recombination. The initial absorbance of the dye cations that were generated within the laser pulse (at $t = 0$) was not reduced at all by the presence of the alumina layer. This indicates that the electron injection yield was not affected at all by the thin layer of Al_2O_3 (with Al/Ti = 0.018). On the other hand, when the barrier layer was much thicker with Al/Ti = 0.18, the dye cations were not generated at all, which indicates that the thick barrier layer prohibited the electron injection from the excited dye. This is fully consistent with the alumina loading dependent activity data shown in Figure 6. Therefore, we conclude that the enhanced sensitized activity of alumina thin layer coated TiO_2 should be attributed to the slower recombination through the alumina barrier layer.

Conclusions

Introducing a thin Al_2O_3 overlayer on the dye-sensitized TiO_2 significantly increased the visible light-sensitized activity for hydrogen production and the degradation of CCl_4. By measuring TDR spectra of bare TiO_2 and Al_2O_3/TiO_2 in slurry, the main role of the alumina barrier layer is proven to retard the charge recombination between the electron injected from the excited dye and the oxidized dye. The yield of the electron injection from the excited dye to TiO_2 CB was little affected by the presence of the alumina thin layer. Although such an approach has been previously demonstrated in a DSSC system, this study shows that a similar approach can be successfully adopted in sensitized photocatalysis. The proposed Al_2O_3/TiO_2/Pt photocatalyst should serve as a model of more practical dye-sensitized photocatalysts.

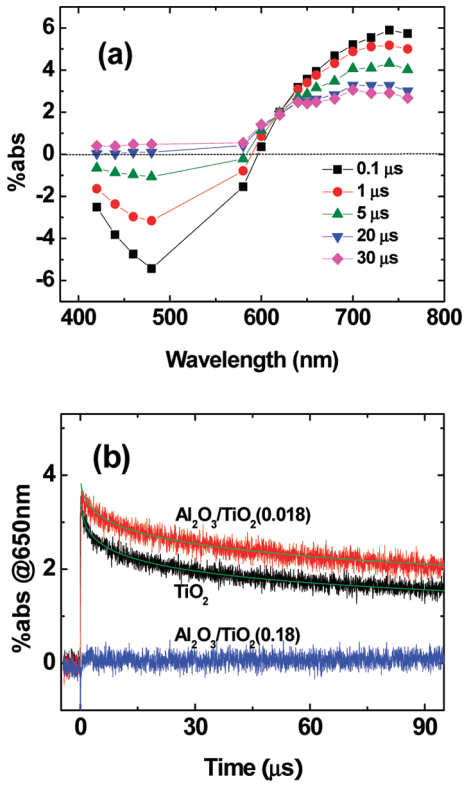

Figure 8. (a) TDR spectra of Al_2O_3/TiO_2 and (b) time traces of absorbance at 650 nm during the 532-nm laser photolysis of dye-sensitized TiO_2 and Al_2O_3/TiO_2 (Al/Ti atomic ratio in parentheses) in slurry. The exponential decay lines in (b) are the results fitted by the stretched exponential function (eq 7). See Table 1 for parameters.

TABLE 1: Kinetic Parameters for the Charge Recombination Processes[a]

	τ (μs)	α
bare TiO_2	80 ± 15	0.23 ± 0.02
Al_2O_3/TiO_2	280 ± 30	0.28 ± 0.02

[a] Obtained by averaging over more than two experiments.

Acknowledgment. This work was supported by a KOSEF grant funded by the Korean government (MEST) (Grant R0A-2008-000-20068-0), the KOSEF EPB center (Grant R11-2008-052-02002), and the Brain Korea 21 program. T.M. and T.T. are grateful for a Grant-in-Aid for Scientific Research (Project Nos. 17105005, 19750115, and others) from the Ministry of Education, Culture, Sports, Science and Technology (MEXT) of the Japanese government.

References and Notes

(1) Grätzel, M. *Acc. Chem. Res.* **1981**, *14*, 376.
(2) Grätzel, M. *Nature* **2001**, *414*, 338.
(3) Kamat, P. V. *J. Phys. Chem. C* **2007**, *111*, 2834.
(4) O'Regan, B.; Grätzel, M. *Nature* **1991**, *353*, 737.
(5) Palomares, E.; Clifford, J. N.; Haque, S. A.; Lutz, T.; Durrant, J. R. *Chem. Commun.* **2002**, 1464.
(6) Palomares, E.; Clifford, J. N.; Haque, S. A.; Luts, T.; Durrant, J. R. *J. Am. Chem. Soc.* **2003**, *125*, 475.
(7) Choi, H.; Kim, S.; Kang, S. O.; Ko, J.; Kang, M.-S.; Clifford, J. N.; Forneli, A.; Palomares, E.; Nazeeruddin, M. K.; Grätzel, M. *Angew. Chem., Int. Ed.* **2008**, *47*, 8259.
(8) Furlong, D. N.; Wells, D.; Sasse, W. H. F. *J. Phys. Chem.* **1986**, *90*, 1107.
(9) Stipkala, J. M.; Castellano, F. N.; Heimer, T. A.; Kelly, C. A.; Livi, K. J. T.; Meyer, G. J. *Chem. Mater.* **1997**, *9*, 2341.
(10) Bae, E.; Choi, W. *J. Phys. Chem. B* **2006**, *110*, 14792.
(11) Park, H.; Choi, W. *Langmuir* **2006**, *22*, 2906.
(12) Zhang, J.; Du, P.; Schneider, J.; Jarosz, P.; Eisenberg, R. *J. Am. Chem. Soc.* **2007**, *129*, 7726.
(13) Cho, Y.; Choi, W.; Lee, C.-H.; Hyeon, T.; Lee, H.-I. *Environ. Sci. Technol.* **2001**, *35*, 996.
(14) Bae, E.; Choi, W.; Park, J.; Shin, H. S.; Kim, S. B.; Lee, J. S. *J. Phys. Chem. B* **2004**, *108*, 14093.
(15) Zhao, J.; Chen, C.; Ma, W. *Top. Catal.* **2005**, *35*, 269.
(16) Zhao, D.; Chen, C.; Wang, Y.; Ma, W.; Zhao, J.; Rajh, T.; Zang, L. *Environ. Sci. Technol.* **2008**, *42*, 308.
(17) Zhao, W.; Sun, Y.; Castellano, F. N. *J. Am. Chem. Soc.* **2008**, *130*, 12566.
(18) Warman, J. M.; de Haas, M. P.; Pichat, P.; Koster, T. P. M.; Van der Zouwen-Assink, E. A.; Mackor, A.; Cooper, R. *Radiat. Phys. Chem.* **1991**, *37*, 433.
(19) Bae, E.; Choi, W. *Environ. Sci. Technol.* **2003**, *37*, 147.
(20) Draper, R. B.; Fox, M. A. *J. Phys. Chem.* **1990**, *94*, 4628.
(21) Tachikawa, T.; Tojo, S.; Kawai, K.; Endo, M.; Fujitsuka, M.; Ohno, T.; Nishijima, K.; Miyamoto, Z.; Majima, T. *J. Phys. Chem. B* **2004**, *108*, 19299.
(22) Tachikawa, T.; Takai, Y.; Tojo, S.; Fujitsuka, M.; Irie, H.; Hashimoto, K.; Majima, T. *J. Phys. Chem. B* **2006**, *110*, 13158.
(23) Tojo, S.; Tachikawa, T.; Fujitsuka, M.; Majima, T. *J. Phys. Chem. C* **2008**, *112*, 14948.
(24) Kraeutler, B.; Bard, A. J. *J. Am. Chem. Soc.* **1978**, *100*, 4317.
(25) Lee, J.; Choi, W. *Environ. Sci. Technol.* **2004**, *38*, 4026.
(26) Park, H.; Choi, W. *J. Phys. Chem. B.* **2004**, *108*, 4086.

(27) Moulder, J. F.; Stickle, W. F.; Sobl, P. E.; Bomben, K. D. *Handbook of X-ray Photoelectron Spectroscopy*; Perkin-Elmer: Eden Prairie, MN, 1992.
(28) Yoshihara, T.; Katoh, R.; Furube, A.; Tamaki, Y.; Murai, M.; Hara, K.; Murata, S.; Arakawa, H.; Tachiya, M. *J. Phys. Chem. B* **2004**, *108*, 3817.
(29) Yoshihara, T.; Tamaki, Y.; Furube, A.; Murai, M.; Hara, K.; Katoh, R. *Chem. Phys. Lett.* **2007**, *438*, 268.
(30) Zhang, J. Z. *J. Phys. Chem. B* **2000**, *104*, 7239.
(31) Tang, J.; Durrant, J. R.; Klug, D. R. *J. Am. Chem. Soc.* **2008**, *130*, 13885.
(32) Vinodgopal, K.; Hua, X.; Dahlgren, R. L.; Lappin, A. G.; Patterson, L. K.; Kamat, P. V. *J. Phys. Chem. B* **1995**, *99*, 10883.
(33) Fitzmauice, D. J.; Frei, H. *Langmuir* **1997**, *7*, 1129.
(34) Clifford, J. N.; Palomares, E.; Nazeeruddin, M. K.; Grätzel, M.; Nelson, J.; Li, X.; Long, N. J.; Durrant, J. R. *J. Am. Chem. Soc.* **2004**, *126*, 5225.

JP9008114